# Journal of Materials Chemistry C

Accepted Manuscript


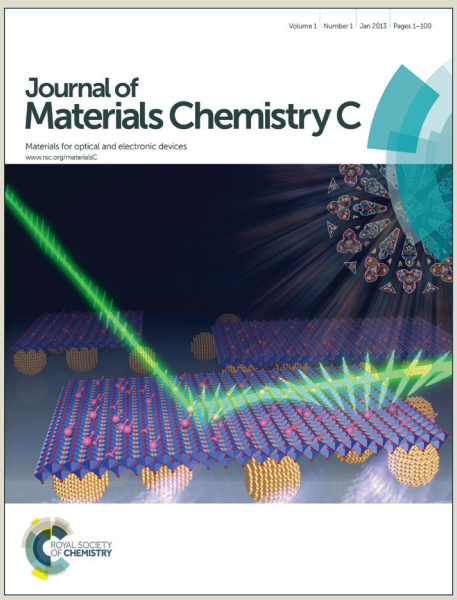





ROYAL SOCIETY OF CHEMISTRY

www.rsc.org/materialsC

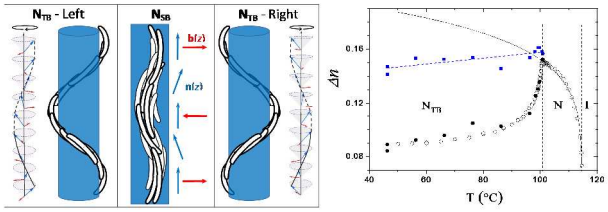


Precise birefringence measurements in large monodomains of the twist-bend nematic phase strongly support its heliconical structure and doubly degenerate handedness.

Cite this: DOI: 10.1039/c0xx00000x

www.rsc.org/xxxxxx

ARTICLE TYPE

# The Temperature Dependence of the Heliconical Tilt Angle in the Twist-Bend Nematic Phase of the Odd Dimer CB7CB

**C. Meyer,[a] G. R. Luckhurst,[b] and I. Dozov[a,*]**

***Received (in XXX, XXX) Xth XXXXXXXXX 20XX, Accepted Xth XXXXXXXXX 20XX***
**DOI: 10.1039/b000000x**

We report precise birefringence measurements in the nematic, N, and in the twist-bend nematic, $N_{TB}$, phases of the odd liquid crystal dimer CB7CB. The birefringence results obtained in large monodomains of the $N_{TB}$ phase strongly support its heliconical structure with doubly degenerate handedness and provide the temperature dependence of the conical tilt angle $\theta$. The birefringence measured in the planar wall defects separating the monodomains with opposite sign of the chirality suggests a splay-bend structure of the nematic in this region, enabling a smooth transition between the adjacent right- and left-handed heliconical domains.

## Introduction

The liquid crystal (LC) materials are well-known for their extraordinary electro-optical properties, leading to numerous technological applications. The now omnipresent liquid crystal displays (LCD) use mainly the nematic phase, the simplest LC phase exhibiting only orientational order: the elongated nematic molecules have no long-range positional order, but are, on average, parallel to the nematic director **n**, the macroscopic symmetry axis of the phase. When composed of achiral molecules, the nematic phase (N) is achiral, and the director remains uniform throughout the sample in the absence of external forces. When the molecules are chiral, the nematic phase is also chiral (N*, chiral nematic or cholesteric phase) and the director **n** is spontaneously twisted, forming a helix with the director perpendicular to the helix axis. Other LC phases, with more complex organization and lower macroscopic symmetry, e.g. the chiral smectic phases, are also promising for applications due to their spontaneous polarization and strong coupling with applied electric fields. However, because of the positional order of the smectic phases, it is difficult to obtain (and to keep under strong fields) well-aligned textures, usually needed for LCD displays.

Although most mesogenic molecules have rod-like or possibly disc-like shapes, less symmetric molecules may also exhibit LC phases. Bent-shape molecules have attracted attention long ago[1] in the nematic phase with their flexoelectric properties. More recently, the discovery[2, 3] of chiral smectic phases composed of achiral bent-shape molecules further increased the interest in these low-symmetry mesogenic molecules, especially because of their strong spontaneous polarization. Nematic phases of strongly bent-shape achiral molecules have also been reported[4-10] to exhibit doubly degenerate chiral domains, textures similar to the usual smectic and chiral-nematic focal conics, and nematic-nematic transitions. All of these features suggest the existence of a new nematic phase for bent-shape mesogenic molecules, similar to the theoretically predicted[11-15] twist-bend phase, $N_{TB}$. In this phase, the bent-shape mesogenic molecules have long-range orientational order as in usual nematics, and no long-range positional order. However, the equilibrium state of the twist-bend nematic is not uniform, but spontaneously bent, with the precession of the director on a conical helix[14] with a short pitch $P_s$ and aperture angle $\theta$, $\mathbf{n}(Z) = (\sin\theta\cos\varphi, \sin\theta\sin\varphi, \cos\theta)$. Here **Z** is parallel to the helix axis and $\varphi = \mathbf{q}\cdot\mathbf{Z}$, where the wave vector **q** of the director distortion is parallel to **Z** and is related to the spontaneous pitch $P_s$ by $|\mathbf{q}| = q = \pm 2\pi / P_s$. The chiral symmetry of the $N_{TB}$ phase is broken and the ground-state has doubly degenerate handedness (see Fig. 1), with twin domains of opposite twist $t = \mathbf{n}\cdot(\nabla\times\mathbf{n}) = -q\sin^2\theta$.

Qualitatively, the expected $N_{TB}$ structure has been clearly confirmed by a large number of different experimental techniques for the lower-temperature nematic phase of the bent-shape mesogenic odd dimer CB7CB[10]. In particular, the "signature" of the $N_{TB}$ phase, the doubly degenerate chirality, is apparent from optical and NMR measurements. Later, large coexisting single domains with alternating handedness were reported in an electro-optic experiment with the same dimer[16], and the spontaneous pitch was estimated to be about 7 nm. Direct freeze fracture experiments[17, 18] rapidly confirmed this extremely short value for CB7CB, and reported similar values for other twist-bend nematics. An even smaller value, of about 5 nm, was determined for $P_s$ from the deuterium quadrupolar splittings of the mesogenic probe, 8CB-$d_2$ dissolved in the twist-bend nematic phase of CB7CB[22] by using a molecular field based model[19].

Two different mechanisms have been proposed to induce the $N_{TB}$ phase. Meyer[11], and later Lorman and Mettout[12], suggested that the $N_{TB}$ structure arises due to a spontaneous macroscopic polarization of the nematic (ferroelectric, anti-ferroelectric, or heli-electric). Alternatively, Dozov[14] described the $N_{TB}$ phase as a

purely elastic instability of the bent-shape anisotropic fluid, and independently Memmer[15] arrived at the same conclusion by Monte Carlo simulations. The main mechanism responsible for the $N_{TB}$ phase is still an open question, although some of the experimental observations are in good agreement with the predictions of the "negative elasticity" model[14]: the extremely short pitch, its strikingly precise estimation based on the elastic instability model, the unusual theoretically calculated[10, 20] and experimentally measured[21] decrease of the bend elastic constant $K_3$ with decreasing temperature in the high-temperature nematic phase.

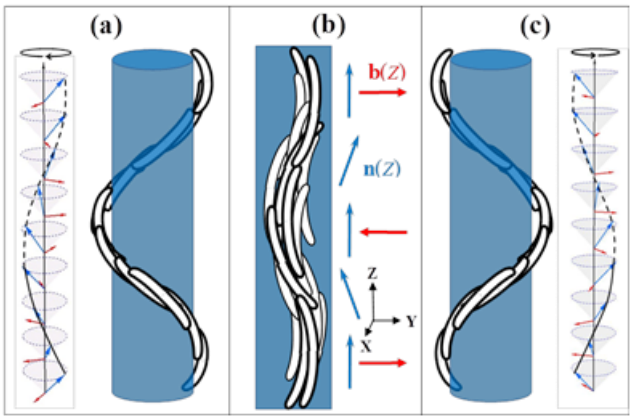


**Fig. 1** Structure of the twist-bend, $N_{TB}$, and splay-bend, $N_{SB}$, nematic phases for bent-shape mesogenic molecules. The director **n** and the bend vector $\mathbf{b}=\mathbf{n}\times(\nabla\times\mathbf{n})$ are shown respectively with blue and red arrows: (a) and (c) Single-domains of the $N_{TB}$ phase with respectively left and right handedness. The director is spontaneously distorted, forming a conical twist-bend helix with aperture angle $\theta_{TB} < \pi/2$ and extremely short pitch of about 10 nm; (b) In the $N_{SB}$ phase the director oscillates in a random distribution of planes, with angular amplitude $\theta_{SB} < \pi/2$. This achiral spontaneously distorted splay-bend structure also has an extremely short period, similar to that for $N_{TB}$.

One obvious way to identify clearly the physical mechanism responsible for the $N_{TB}$ phase and to improve further its theoretical description is the experimental measurement of the main structural parameters of the phase, the pitch $P_s$ and the tilt angle of the conical helix $\theta$, as a function of the temperature. Recent experiments provided indirect electro-optical estimation[16] and direct measurement[17, 18] for the pitch in CB7CB and other bent-shaped mesogenic molecules. In principle, quite direct measurement is also possible for the tilt angle $\theta$, from a study of the temperature dependence of the average birefringence[14, 16] in the short-pitch $N_{TB}$ phase. However, due to the difficulty of obtaining sufficiently large and uniform $N_{TB}$ textures, so far only approximate values, and in a narrow temperature window, have been reported for $\theta$ from birefringence measurements[17]. However, Chen et al.[17] also noted that although their birefringence measurements were consistent with the deuterium quadrupolar splittings for a mesogenic monomer dissolved in CB7CB[22] for the nematic phase this was not the case for the results in the twist-bend nematic phase. We have noticed similar behavior for our detailed birefringence of CB7CB and the extensive measures of the quadrupolar splittings for CB7CB-$d_4$[10]. That is the results for the two techniques are consistent in the nematic but not the twist-bend nematic. We have yet to find a satisfactory explanation for this difference.

Here we present a precise experimental measurement of the birefringence $\Delta n$ in the N and $N_{TB}$ phases of CB7CB, providing the temperature dependence of the spontaneous tilt angle $\theta$ of the $N_{TB}$ conical helix. In a thin cell we achieve alternating uniform single-domains of the two doubly degenerate $N_{TB}$ conical helices with opposite handedness, separated by domain walls. Comparing the $N_{TB}$ birefringence data with the $\Delta n(T)$ dependence extrapolated from the high-temperature nematic phase, we find that the tilt angle increases from $\theta \approx 9°$ at the N - $N_{TB}$ transition temperature, up to an almost saturated value of $\theta \approx 37°$ at 50 ºC below the transition. Our $\Delta n$ data measured in the domain walls suggest a splay-bend structure of the wall, due to the constraint imposed by the adjacent single domains having opposite-handedness.

## Materials and methods

**Twist-bend nematic CB7CB**: The chemical structure of the liquid crystal dimer, CB7CB (see Figure 2) consists of two cyanobiphenyl mesogenic groups, linked by a heptane spacer; its systematic name is 1",7"-bis(4-cyanobiphenyl-4'-yl)heptane. In our experiments the first-order nematic-isotropic transition occurs at 114.6 ºC, the twist-bend nematic-nematic transition is also first order and occurs at $T_{NtbN} \approx 100.8$ °C, with about 1 °C of hysteresis and coexistence of the two nematic phases; the melting point is $T_{CrNtb}$=102 ºC, but the twist-bend nematic phase can be supercooled to about 31 ºC[10]. The heptane spacer is shown on Figure 2 in its all-trans conformation, giving the bent-shape of this conformer. A large number of other conformers exist, but most of them are also bent, so the average conformation of the dimer is also bent-shape[23].

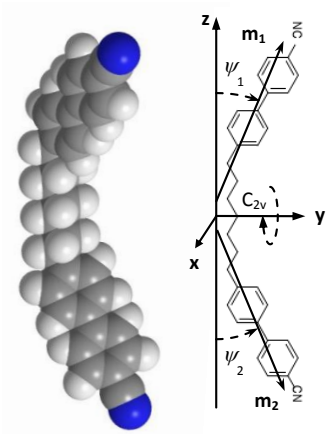


**Fig. 2** Schematic representation of the molecule of the CB7CB dimer in its all-trans conformation. The two monomers, similar to 3CB molecules, lie in the **yz** plane. The main axes of the two monomers, $\mathbf{m}_1$ and $\mathbf{m}_2$, directed approximately along the cyanobiphenyl para-axes, are oriented at angles $\psi_1=\psi_2$ with respect to the long axis, **z**, of the molecule. The **y**-axis is approximately a $C_{2v}$ symmetry axis of this conformer.

**Experimental cells:** In the main experiment we have used a sandwich cell, prepared from two ITO covered glass plates, separated with 1.5 µm silica balls as spacers. Prior to the experiments, the cell gap, $d$, was measured interferometrically to be 1.6 ±0.1 µm. The ITO electrodes were covered with a polymer alignment layer, rubbed unidirectionally to align the director for the nematic phase parallel to the **Z**-axis of the laboratory frame

(in the plane of the cell, see Figure 3). The cell was filled by capillarity with CB7CB in the isotropic phase, at T=125°C.

In additional experiments, in order to confirm the absolute value of the measured birefringence, a different kind of cell was used. This "spherical-wedge" cell is made with one flat plate and one spherical convex glass lens with a curvature radius, *R*, of 50 mm. To create a uniform alignment of the nematic, the inner surfaces of the two substrates were treated respectively with a unidirectionally rubbed Nylon layer and by SiO oblique evaporation.

**Measurement setup and techniques:** For texture observations and electro-optic measurements the cell was placed in a heating stage (Instec) mounted on a polarizing microscope (Leitz Ortholux). The microscope is equipped with a Berek tilting compensator (Leitz) and with a digital camera (Dino-lite Pro AM423X). For precise measurement of the transmitted intensity, a microphotometer (D-104, PTI) is mounted on the microscope, enabling us to measure the intensity locally, inside a small rectangular window in the image plane of the microscope, corresponding to an area of 10×10 μm$^2$ in the sample.

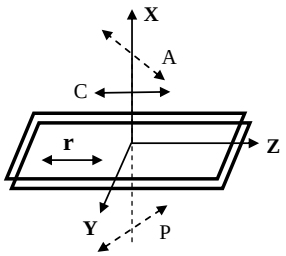


**Fig. 3** Geometry of the birefringence measurements and orientation of the thin sandwich cell in the laboratory frame **XYZ**. The rubbing direction, **r**, parallel to the **Z**-axis, defines the preferred orientation of the director **n** in the nematic phase and of the helix axis in the $N_{TB}$ phase. In both cases the optical axis of the sample is parallel to **Z** and to the rapid axis of the compensator C. The sample is observed along the **X**-axis under crossed polarizers, P and A, rotated at ± 45° with respect to **r**.

Three different techniques have been used for the birefringence measurement. The first is the direct measurement of the total phase-shift $d.\Delta n$ in the cell, compensating it with the Berek compensator under crossed polarizers. A great advantage of this method is that it is very direct, based only on the position of the tilt of the compensator plate for which the transmitted intensity is minimized, and not to the absolute value of the intensity. Then, this technique can be applied to measure $\Delta n$ even in regions where it rapidly varies with position, on the scale of a few μm, which is the case in the defect walls separating the single domains. However, the precision of the identification of the intensity minimum is low and the error in the measurement of $d.\Delta n$ is relatively high, about 6 nm. Therefore, we used this technique only for the measurements in the defect walls, too thin for the other measurement techniques (at the N-$N_{TB}$ transition the wall thickness is about 1μm, it increases with decreasing temperature, attaining 5 μm deep into the $N_{TB}$ phase, see Fig. 4), where other techniques cannot be applied. Moreover, the absolute value of $\Delta n$ depends on the precision of the measurement of the cell thickness (see later).

The second technique, requiring larger uniform regions, has been applied in the monochiral domains of the $N_{TB}$ phase. In this case we again use the Berek compensator, but instead of the qualitative measurement of the position of the minimum, we measure quantitatively the transmitted intensity with the microphotometer for a few points around the minimum. Fitting the data with a parabola, we obtain the value of the phase-shift with much better precision, typically with error bars as low as 0.4 nm. However, the absolute value of $\Delta n$ depends again on the precision of the measurement of the cell gap *d*.

It should be noted, that despite the measurement of *d* in the empty cell before the experiment, this value can vary, in principle, during the experiment. In fact, in such thin cells the capillary pressure after filling the cell might lead to deformation of the glass plates and up to 10 % variation in *d*. In addition, when the cell is heated to 100-120 °C during the experiment, additional deformations can result, due to the temperature-induced variation of all the mechanical properties of the plates and the polymer walls of the cell. This artefact is particularly dangerous in our case, as it depends on the cell history and/or on the temperature, i.e. it will not simply multiply the $\Delta n$ results by a constant factor, but will change the $\Delta n(T)$ dependence, affecting seriously the data interpretation. To confirm that *d* does not vary with temperature, we measured $\Delta n(T)$ directly in a separate experiment for the nematic phase of CB7CB. In the spherical-wedge cell, the local gap $d(r)$ varies continuously with the distance *r* from the point of contact of the two substrates. Comparing the interference picture taken under polarizers crossed at 45° with respect to the alignment direction, with that expected theoretically, we obtain the temperature dependence of $\Delta n$ in the nematic phase. Comparison with the more precise results for $d.\Delta n$ from the main experiment confirms that the cell gap is independent of the temperature, $d = 1.61 \pm 0.02$ μm, throughout the nematic phase. We note, that this direct technique cannot be applied in the $N_{TB}$ phase, because it requires a good planar alignment up to local gap values $d(r) \approx 10$ μm, achieving this seems not to be possible in the twist-bend nematic.

## Experimental Results

**Qualitative observations:** After filling the 1.6 μm cell with CB7CB in the isotropic phase and equilibration for 30 min, the temperature was slowly decreased to the transition to the high-temperature (standard) nematic phase N, taking place at $T_{NI}$= 114.6 °C. The nematic director **n** was uniform and parallel to the rubbing direction **Z** of the alignment layers. The usual electro-optic effects, like the Fréedericksz transition[24] and the flexoelectric Bobylev-Pikin instability [25], confirmed the standard nematic behaviour of the observed N phase.

On decreasing the temperature further, we observe the transition to the $N_{TB}$ phase, at $T_{NtbN}$ =100.8 °C. As already reported [10], this transition is weakly first order, with about 1°C of hysteresis, and a coexistence range of about 0.2 °C for very slow temperature variation. For a slow cooling rate of 0.1 °C/min, the $N_{TB}$ phase nucleates first outside of the field of view, where in the absence of heating by the microscope lamp the temperature is slightly lower. Then the $N_{TB}$ domains grow along the direction **Y**, perpendicular to the director **n** and lying in the plane of the sample. The typical texture at the transition is shown on Fig. 4a: inside the uniform N phase (slightly) less uniform stripes of the $N_{TB}$ phase are seen to grow. On further cooling, the growing stripes occupy most of the field of view, separated by thin

nematic regions. Progressively merging, the stripes organize into much larger bands (see Fig. 4b-4e), separated by thin walls. The nematic regions disappear and the whole sample is now in the $N_{TB}$ phase.

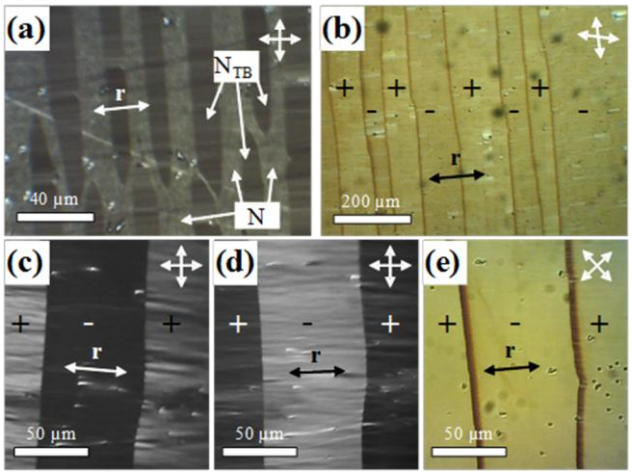


**Fig. 4** Quasi-uniform textures in the $N_{TB}$ phase of CB7CB as observed by polarized optical microscopy (POM) in a 1.6 µm thin cell. The double-headed white arrows show the orientation of the polarizers and **r** marks the rubbing direction. The single-domains with alternating sign of the chirality in (b) - (e) are marked with + and - . The alternation of the handedness is verified by electroclinic measurements[16]: (a) Growth of thin domains of the $N_{TB}$ phase inside the high-temperature standard N phase at $T = T_{NtbN} = 100.8$ °C; (b) Single domains separated by domain walls at $T$= 95.0 °C. The polarizers are uncrossed by rotation respectively by ± 7°, in order to increase the light transmission; (c) and (d) Inversion of the contrast of the single-domains with alternating handedness upon rotation of the sample under crossed polarizers at $T$= 99.0 °C; (e) Sample rotated at 45° under crossed polarizers at $T$= 50.0 °C. The uniform colors in the adjacent single-domains show that the phase-shift $d.\Delta n$ is uniform and independent of the sign of the chirality of the domain. In the defect walls separating the monodomains the interference colors are different, showing significantly higher birefringence.

The $N_{TB}$ texture shown on Fig. 4 is almost uniform, unlike the usual focal conic, fan shape and other complicated textures usually observed in thicker cells. Indeed, rotating the cell under crossed polarizers, we observe that the in-plane projection of the optic axis **N** of the $N_{TB}$ phase is almost uniform, oriented approximately along the rubbing axis **Z**, with local deviation between **N** and **Z** less than ± 2°. We note that this small deviation, coming from weak smectic-like textural defects, is visible in Figs. 4c and 4d due to the strongly enhanced contrast of the photographs taken under crossed polarizers, respectively parallel and perpendicular to the $N_{TB}$ optic axis. However, in the geometry used for the birefringence measurement, with the crossed polarizers at 45° with respect to the **Z**-axis, the transmitted light intensity is quite uniform, independent of the local alignment defects (see Fig. 4e), resulting in negligibly small errors in the measured birefringence. Rotating the sample at 45° reveals, from the interference colors, that the birefringence is constant throughout the "bands", but is different, slightly higher, in the defect walls. Cooling the sample to 50°C, the texture remains qualitatively the same, but the walls become larger and their birefringence, $\Delta n_W$, remains approximately constant, while the birefringence in the bands, $\Delta n_B$, decreases with decreasing temperature. On repeatedly cooling and heating the sample within the $N_{TB}$ phase, no hysteresis is observed in the $\Delta n$ variation.

When heating to the N phase and slowly cooling back to the $N_{TB}$ phase, we observe qualitatively the same texture, a series of bands parallel to the **Y** axis, separated by walls, although the bands and the walls are not at the same positions.

The observed features are compatible with the expected heliconical structure of the $N_{TB}$ phase. Indeed, due to the extremely short pitch, $P_s << \lambda$ ($\lambda$=546 nm in our experiment), the $N_{TB}$ phase is expected to be optically uniaxial[16], with the optic axis **N** along the average direction of **n**, i.e. along the helix axis. In the nematic phase the director **n** is oriented, at the surfaces, along the rubbing direction **r**. In the $N_{TB}$ phase, due to its heliconical structure and to the finite anchoring strength, the surface director deviates locally from **r**. However, the optic axis **N**, which is defined as the macroscopic average of **n**, is still expected to be oriented along **r**[16]. Indeed, throughout the $N_{TB}$ phase we observe that the optic axis **N** remains uniform, with only small local deviations from **r** in both the monodomains and the defect walls between them.

For the same reason, namely $P_s << \lambda$, the optical activity is expected to be too small to be observed in such a thin cell, despite the chiral symmetry breaking in the $N_{TB}$ phase. However, under slightly uncrossed polarizers, the observed contrast alternates from one band to the next one, and a detailed electro-optic study[16] demonstrated, that the bands are in fact large monochiral single-domains of the $N_{TB}$ phase, with alternating handedness. The walls can be then identified as the expected[14] defect walls separating regions of opposite chirality.

The decrease of $\Delta n$ with decreasing temperature is also expected [14, 18] in the monochiral domains of the $N_{TB}$ phase. Indeed, due to the short pitch, the effective $N_{TB}$ phase refractive indices are the average over one period of the local refractive indices in the director frame, precessing around the optic axis **N**. Naturally, the measured average birefringence is smaller than the local one, due to the tilt angle of **n** with respect to **N** (for more details see the model section given later).

**Temperature Dependence of the Birefringence:** The main birefringence results are presented on Fig. 5. These data, measured in several independent heating and cooling runs, show excellent reversibility and are completely hysteresis-free. This behavior confirms that both the N and $N_{TB}$ phases are in thermal equilibrium throughout the experiment. In particular, these results strongly support the fluid nematic nature of the $N_{TB}$ phase of CB7CB, as opposed to the recently suggested[26] "glassy nematic" and "soft crystal" states formed by the similar, bent-shaped mesogenic compound CB11CB. In the N phase the birefringence, $\Delta n_N$, has the usual nematic behavior, rapidly increasing with decreasing temperature. The data are well-fitted with the classical Haller formula[27] $\Delta n = \Delta n_0 ( 1 - T / T^* )^{\beta}$, with $\beta \cong 0.139$ and $T^* \cong$ 114.5 °C corresponding to the N-I phase transition temperature. Here $\Delta n_0 \cong 0.240$ is the birefringence extrapolated to absolute zero, when the order parameter $S$ saturates to 1. Here we use for the dimer order parameter the standard definition $S = \langle 3(\mathbf{n}.\mathbf{z})^2 - 1 \rangle / 2$, valid in both the N and $N_{TB}$ phases (*n.b.* that in the $N_{TB}$ phase the director **n** is uniformly distributed around the optic axis **N**, tilted at the angle $\theta$, while in the N phase **n** coincides with **N**). The extrapolation of the Haller fit in the $N_{TB}$ phase gives the expected birefringence behavior, under the assumption that $S$ is continuous at the transition and the conical

tilt angle $\theta$ is zero here, or negligibly small.

Below the transition temperature, the observed behavior of the birefringence $\Delta n_B$ in the single-domains is drastically different. At the transition, the birefringence slightly increases, with a jump of $\delta n_B = \Delta n_B - \Delta n_N = 0.0034$, this is quite small but still observable. We note that a finite jump $\delta\theta \neq 0$ of the $N_{TB}$ conical tilt angle at the transition can only decrease the birefringence, leading to $\delta n_B < 0$. So, the observed positive jump $\delta n_B > 0$ indicates an increase $\delta S = S^{TB} - S^{N}$ of the nematic order parameter in the lower temperature $N_{TB}$ phase, compatible with a weak first-order phase transition.

Below the transition, $\Delta n_B$ first decreases rapidly and then almost saturates at very low temperatures. Taking into account that no texture changes are observed and that the optic axis, **N**, remains parallel to the rubbing direction **r**, this behavior confirms the predicted[14] increase of the conical tilt angle $\theta$ with decreasing temperature. Moreover, comparing the temperature dependence of $\Delta n_B$ with the extrapolated $\Delta n_N$ curve, we can conclude that $\theta$ attains quite high values at low temperature.

Qualitatively different behavior is observed for the birefringence in the walls separating the single domains of the $N_{TB}$ phase. The jump of $\Delta n_W$ at the transition, $\delta n_W = \Delta n_W - \Delta n_N = 0.0076$, is positive and higher than $\delta n_B$, showing again an increase of the order parameter $S$ in the $N_{TB}$ phase, with respect to the $S$-value in the nematic phase. With the reasonable assumption that $S$ is not significantly different in the walls and in the bands, from $\delta n_W > \delta n_B$ we can qualitatively conclude that the tilt of the local director **n** in respect to the optic axis **N** is higher in the bands, than in the walls between them. Throughout the $N_{TB}$ phase, $\Delta n_W$ varies very slowly, with only a minor decrease at lower temperature. This behavior, which is drastically different from both $\Delta n_B$ and the extrapolated $\Delta n_N$ data, shows that the structure of the domain wall is neither the same as the $N_{TB}$ phase monodomain, nor that of the standard nematic phase.

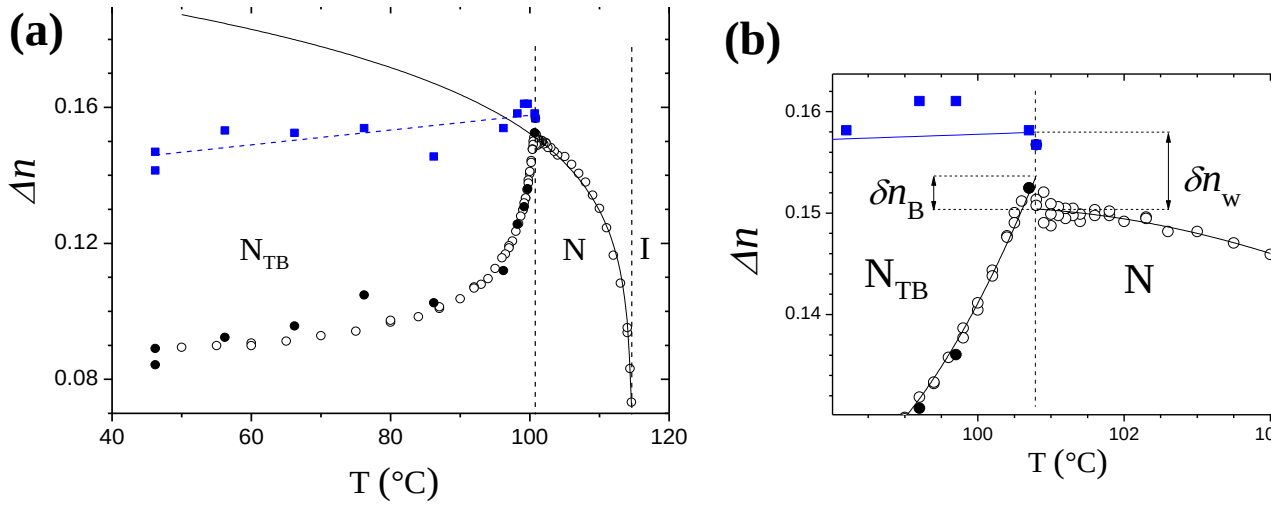


**Fig. 5** Temperature dependence of the birefringence in the nematic and the $N_{TB}$ phases of CB7CB. (a) Whole set of data obtained in several cooling and heating runs. The open symbols are from the precise microphotometer measurements, the full symbols are the data from the less precise direct Berek compensator measurements. In the $N_{TB}$ phase, the circles refer to the birefringence measured in the bands, $\Delta n_B$, while the squares correspond to the birefringence in the walls, $\Delta n_W$. The continuous line is the Haller extrapolation from the data in the N phase, $\Delta n_N$; the dashed line is a linear fit of the $\Delta n_W$ data. (b) Zoom of the birefringence in the vicinity of the $N_{TB}$-N phase transition. The symbols are the same as before, and the lines are polynomial fits of each data set, in order to extrapolate the birefringence values at the N-$N_{TB}$ transition and to obtain the birefringence jumps in the walls, $\delta n_W = \Delta n_W - \Delta n_N = 0.0076$, and in the bands, $\delta n_B = \Delta n_B - \Delta n_N = 0.0034$.

## Theoretical Model and Discussion

### Heliconical tilt in the $N_{TB}$ phase

To calculate the refractive indices, we need first to find the macroscopic average $\langle \boldsymbol{\alpha} \rangle$ of the molecular polarizability tensor, $\boldsymbol{\alpha}$. Here the brackets denote an average with the appropriate orientational distribution function (ODF), describing the orientation of the molecules in the reference frame **123** related to the nematic director **n**. In the standard N phase, the ODF is uniaxial, while in the $N_{TB}$ phase it is biaxial[14, 28]. However, due to the small pitch in comparison with the wavelength of light all of the optical properties in the $N_{TB}$ phase should be additionally averaged over one period of the helix; this second average will be denoted by a bar over the averaged expression, e.g. $\overline{\langle \boldsymbol{\alpha} \rangle}$.

To a first approximation and for an average over all of the molecular conformations, the CB7CB dimer is biaxial; it may be thought of as consisting of two alkyl-cyanobiphenyl monomers, rigidly attached to one another (see Fig. 2b). To a reasonable approximation, each one of the two monomers is rod-like, with the long axis of its polarizability tensor $\boldsymbol{\alpha}^m$ at an angle $\psi$ with respect to the long axis **z** of the dimer. In the absence of conjugated bonds between the monomers, the polarizability is essentially additive, and we obtain for the dimer $\boldsymbol{\alpha} = \boldsymbol{\alpha}^{m1} + \boldsymbol{\alpha}^{m2}$. In the molecular frame **xyz**, the dimer polarizability tensor is

$$\boldsymbol{\alpha} = 2\begin{pmatrix} \alpha_\perp^m & 0 & 0 \\ 0 & \alpha_\perp^m + \Delta\alpha^m \sin^2\psi & 0 \\ 0 & 0 & \alpha_\perp^m + \Delta\alpha^m \cos^2\psi \end{pmatrix}, \qquad (1)$$

in terms of the principal values of the monomer polarizability, $\alpha_\perp^m$ and $\alpha_\parallel^m$, and its anisotropy, $\Delta\alpha^m = \alpha_\parallel^m - \alpha_\perp^m$.

Despite the molecular biaxiality, the conventional nematic phase N is uniaxial, with rotational symmetry around the director **n**. We

choose the director frame of reference **123** with the **3**-axis parallel to the director **n** and the **2**-axis parallel to the preferred average orientation of the **y**-axis of the dimer reference frame. In the nematic phase the **3**-axis coincides with the **Z**-axis of the laboratory frame, and due to the uniaxial symmetry of the phase the **2**-axis can be selected parallel to the **Y**-axis, without any loss of generality. So, in the N-phase the **123** and the **XYZ** frames are identical, while in the locally biaxial $N_{TB}$-phase the director is distributed around **Z** and is defined by the Euler angles ($\varphi$, $\theta$, 0). In the director frame of reference **123**, we can write for the average polarizability tensor in the nematic phase

$$\boldsymbol{\alpha}^{N} = \begin{pmatrix} \alpha_{\perp}^{N} & 0 & 0 \\ 0 & \alpha_{\perp}^{N} & 0 \\ 0 & 0 & \alpha_{\parallel}^{N} \end{pmatrix} = \langle \boldsymbol{\alpha} \rangle , \qquad (2)$$

where the brackets denote the average taken with the nematic ODF, $f$ ($\alpha$,$\beta$,$\gamma$), and ($\alpha$,$\beta$,$\gamma$) are the Euler angles describing the orientation of the dimer frame **xyz** with respect to the director frame **123**. Straightforward calculation gives

$$\alpha_{\perp}^{N} = 2\alpha_{0}^{m} - \frac{1}{3}\Delta\alpha^{m}\left[ S\left(3\cos^{2}\psi - 1\right) + D\sin^{2}\psi \right], \qquad (3)$$

$$\alpha_{\parallel}^{N} = 2\alpha_{0}^{m} + \frac{2}{3}\Delta\alpha^{m}\left[ S\left(3\cos^{2}\psi - 1\right) + D\sin^{2}\psi \right],$$

where $\alpha_{0}^{m} = (\alpha_{\parallel}^{m} + 2\alpha_{\perp}^{m})/3$ is the scalar component of the polarizability of the monomer. Here $S = \langle 3\cos^{2}\beta - 1 \rangle / 2$ is the usual major order parameter for a rod-like molecule (when needed, we will use the notation $S^{N}$ in the nematic phase, to make the distinction with the order parameter $S^{TB}$ in the $N_{TB}$ phase), and $D = 3\langle \sin^{2}\beta \cos(2\gamma) \rangle / 2$ is the biaxial order parameter for a uniaxial nematic comprised of biaxial molecules[29, 30]; in terms of the Saupe ordering matrix[31, 32] these spherical components are $S = S_{zz}^{33}$ and $D = S_{xx}^{33} - S_{yy}^{33}$ [33, 34]. Strictly speaking, the birefringence experiment is not sufficient, as it only gives information about the polarizability anisotropy,

$$\Delta\alpha^{N} = \alpha_{\parallel}^{N} - \alpha_{\perp}^{N} = \Delta\alpha^{m}\left[ S\left(3\cos^{2}\psi - 1\right) + D\sin^{2}\psi \right], \qquad (4)$$

which is a function of the two independent order parameters $S$ and $D$. However, in the absence of experimental data for $S$ and $D$ from other techniques, e.g. from NMR, EPR or Raman measurements, a necessary approximation is to neglect the $D$-term in Eq.(4). Indeed, $D$ is expected to vary as $S(1-S)$ and to be small[29]. For $S \approx 0.63$ at the $N_{TB}$/N phase transition (obtained from the Haller extrapolation procedure and plotted in Fig. 5), we expect $D << S$. Moreover, a rough estimation of the angle $\psi$ from the molecular structure gives $\sin\psi \approx 0.5$, and so the coefficient of the $D$-term in Eq.(4) is one order of magnitude smaller than that for the coefficient of the $S$-term. Neglecting $D$, we obtain

$$\Delta\alpha^{N}(T) \approx \Delta\alpha^{m}\left(3\cos^{2}\psi - 1\right) S^{N}(T) \approx \Delta\alpha_{0}^{N} S^{N}(T), \qquad (5)$$

where $\Delta\alpha_{0}^{N}$ is the $\Delta\alpha^{N}$ value extrapolated to 0 K, where $S^{N}$=1.

To calculate the polarizability tensor of the twist-bend nematic in the rotating director frame, we first need to take an orientational average. However, in this case the local ODF is biaxial: the $C_{2v}$ symmetry axis of the dimer, parallel to the molecular **y**-axis, is preferentially aligned along the **2**-axis of the director frame, selected parallel to the local macroscopic $C_{2v}$ symmetry axis, coinciding with the bend vector $\mathbf{b} = \mathbf{n} \times (\nabla \times \mathbf{n})$. In this way, the curvature of the bent-shaped molecule matches in the best possible way the curvature of the director field. Strictly speaking, the polarizability tensor is biaxial in the rotating director frame,

$$\langle \boldsymbol{\alpha} \rangle^{TB} = \begin{pmatrix} \alpha_{11}^{TB} & 0 & 0 \\ 0 & \alpha_{22}^{TB} & 0 \\ 0 & 0 & \alpha_{33}^{TB} \end{pmatrix}, \qquad (6)$$

and its main values $\alpha_{ii}^{TB}$ are a function of four principal order parameters, usually denoted as $S$, $D$, $P$ and $C$[30, 33]. However, in a similar way as for the nematic phase, the usual order parameter $S$ is expected to be much larger than the order parameters related to the microscopic and macroscopic biaxiality. For symmetry reasons, the macroscopic biaxial order parameters $P$ and $C$ should vanish in the standard N-phase, where $\theta$=0, and are then expected to be proportional to $\theta^{2}$ in the $N_{TB}$ phase. Close to the $N_{TB}$ – N phase transition they can be neglected because of the small value of the heliconical angle, $\theta \approx 10°$ (see later). For simplicity, we will then approximate the local polarizability tensor in the $N_{TB}$ phase as uniaxial,

$$\langle \boldsymbol{\alpha} \rangle^{TB} = \begin{pmatrix} \alpha_{\perp}^{TB} & 0 & 0 \\ 0 & \alpha_{\perp}^{TB} & 0 \\ 0 & 0 & \alpha_{\parallel}^{TB} \end{pmatrix}, \qquad (7)$$

where the principal values are similar to those for the nematic case, but renormalized with the order parameter $S^{TB}$ instead of $S^{N}$. For the anisotropy of the polarizability, in the rotating **123** frame, we obtain then

$$\langle \Delta\alpha \rangle^{TB}(T) \approx \Delta\alpha^{m}\left(3\cos^{2}\psi - 1\right) S^{TB}(T) \approx \Delta\alpha_{0}^{N} S^{TB}(T). \qquad (8)$$

Finally, to obtain the polarizability tensor in the laboratory frame, **XYZ**, we need to average Eq. (8) over one period of the twist-bend helix, taking into account the precession of the director frame **123** with respect to **XYZ**, described by the Euler angles ($\varphi$, $\theta$, 0). As $\varphi = qZ$ and the pitch $P = 2\pi/q$ is much larger than the wavelength of the visible light $\lambda$, we obtain

Cite this: DOI: 10.1039/c0xx00000x

www.rsc.org/xxxxxx

ARTICLE TYPE

$$\overline{\langle \boldsymbol{\alpha} \rangle}^{\mathrm{TB}} \approx \begin{pmatrix} \alpha_{\perp}^{\mathrm{TB}} + \frac{1}{2}\left(\alpha_{\parallel}^{\mathrm{TB}} - \alpha_{\perp}^{\mathrm{TB}}\right)\sin^2\theta & 0 & 0 \\ 0 & \alpha_{\perp}^{\mathrm{TB}} + \frac{1}{2}\left(\alpha_{\parallel}^{\mathrm{TB}} - \alpha_{\perp}^{\mathrm{TB}}\right)\sin^2\theta & 0 \\ 0 & 0 & \alpha_{\parallel}^{\mathrm{TB}} - \left(\alpha_{\parallel}^{\mathrm{TB}} - \alpha_{\perp}^{\mathrm{TB}}\right)\sin^2\theta \end{pmatrix}$$

and the relevant anisotropy for the monodomains becomes

$$\overline{\langle \Delta\alpha \rangle}^{\mathrm{TB}}(T) \approx \Delta\alpha_0^{\mathrm{N}} S^{\mathrm{TB}}(T)\left(3\cos^2\theta(T) - 1\right)/2 . \qquad (9)$$

The explicit form of the relation between the calculated anisotropic polarisability, $\Delta\alpha$, and the measured birefringence depends on the local-field anisotropy in the nematic. Here we adopt the simple and widely used interpretation of LC birefringence data, the isotropic local-field model proposed by Vuks[35]. The semi-empirical Vuks formula

$$\frac{n_i^2 - 1}{\langle n^2 \rangle + 2} = \frac{4\pi}{3} N \alpha_i, \qquad i = \parallel, \perp , \qquad (10)$$

where $N$ is the number density and $\langle n^2 \rangle = (n_{\parallel}^2 + 2n_{\perp}^2)/3$, gives the birefringence as

$$\Delta n = \frac{4\pi}{3} \frac{\langle n^2 \rangle + 2}{n_{\parallel} + n_{\perp}} N \Delta\alpha = \frac{4\pi}{3} cN \Delta\alpha , \qquad (11)$$

where $c \approx 1.40$ is approximately a constant factor for the usual range of values of LC refractive indices[36].

To estimate the angle $\psi$ for the dimer CB7CB, we note that its associated monomer is very similar to the classic and well-studied nematogen 5CB. We can then approximate the unknown polarizability of the CB7CB monomer with the one of the 5CB molecule, $\Delta\alpha^{\mathrm{m}}(\mathrm{CB7CB}) = \Delta\alpha\,(5\mathrm{CB})$. Substituting in Eqs. (5) and (11) and taking into account that the 5CB number density, $N$(5CB), is approximately twice the number density of CB7CB, $N$(CB7CB), we obtain for the angle $\psi$ of the CB7CB dimer

$$\frac{1}{2}(3\cos^2\psi - 1) = \frac{\Delta n_0(CB7CB)}{\Delta n_0(5CB)} . \qquad (12)$$

With $\Delta n_0$(CB7CB) = 0.240 from the Haller fit in Fig. 5 for the N phase and $\Delta n_0$(5CB) = 0.371 calculated from the $\Delta n$ data reported for 5CB[37], we obtain $\psi = 29°$. The effective bend angle for the CB7CB dimer, $\pi - 2\psi$, is then about 122°. This value seems reasonable when taking into account that it is an average over a large number of different conformers. Indeed, our result is in excellent agreement with the statistical-mechanical calculations for CB7CB [10, 23, 38], predicting the conformational distribution of the dimer bend angle in the N phase; this is peaked at about 120°.

To estimate the temperature dependence of the heliconical tilt angle $\theta$ in the monodomains we rearrange Eqs. (9) and (11) in the form

$$\Delta n^{\mathrm{TB}}(T) \approx \Delta n_0^{\mathrm{N}} S^{\mathrm{TB}}(T)\left(3\cos^2\theta(T) - 1\right)/2 . \qquad (13)$$

Further assumptions are now needed to obtain the unknown major order parameter, $S^{\mathrm{TB}}(T)$, of the twist-bend nematic phase. As a zero-order approximation we suppose that $S$ is continuous at the $N_{TB}$-N phase transition and $S^{\mathrm{TB}}(T) = S^{\mathrm{N}}{}_{\mathrm{extr}}(T)$ below it, where $S^{\mathrm{N}}{}_{\mathrm{extr}}(T)$ is given for $T < T_{\mathrm{NtbN}}$ by the Haller extrapolation shown in Fig. 5. This approximation is reasonably good if the nematic order parameter is almost saturated at the $N_{TB}$-N phase transition, implying very weak variation with decreasing temperature. However, this is not exact in our case, as is seen from the small *positive* jump in $\Delta n$ for the monodomains at the transition. Indeed, as $\sin^2\theta \geq 0$, we obtain from Eq. (13) the following lower bound for the order parameter jump at the transition: $\delta S^{\mathrm{TB}} = S^{\mathrm{TB}}(T_{\mathrm{NtbN}}) - S^{\mathrm{N}}(T_{\mathrm{NtbN}}) \geq 0.014$. Moreover, the same argument is also valid for the larger birefringence jump measured in the defect walls (see the later discussion). If we suppose that the nematic order parameter $S$ is the same in the monodomains and in the walls, this larger jump of the birefringence results in a larger lower bound for the $S$-jump at the transition, $\delta S^{\mathrm{TB}} \geq 0.032$. This stronger inequality gives us directly a lower bound for the value of the heliconical angle at $T_{\mathrm{NtbN}}$, namely $\theta\,(T_{\mathrm{NtbN}}) \geq 9°$, corresponding to a weak first-order transition in keeping with the small transitional entropy[10]. Finally, to calculate the temperature dependence of the tilt angle $\theta$ in the $N_{TB}$ phase, we suppose that $S^{\mathrm{TB}}(T) = \delta S^{\mathrm{TB}} + S^{\mathrm{N}}{}_{\mathrm{extr}}(T)$, i.e. that the $S^{\mathrm{TB}}(T)$ curve is simply shifted up by $\delta S^{\mathrm{TB}}$ with respect to the temperature dependence extrapolated from the nematic phase. We note that the $\theta(T)$ dependence is only weakly sensitive to this last approximation.

In Fig. 6 we plot the $\theta(T)$ dependence for the $N_{TB}$ phase of CB7CB, calculated from the birefringence measurements in the monodomains. Our results are in qualitative agreement with the scarce data reported so far for CB7CB, estimated either from other birefringence measurements[17, 18] or from the relaxation times of the electroclinic effect[16]. However, because of the almost perfect alignment achieved in the $N_{TB}$ phase, our results are quite direct, precise and cover a very large temperature range. Despite the number of assumptions in the analysis of the data, $\theta(T)$ is only weakly sensitive to the approximations adopted and we expect it to be quantitatively, or at least semi-quantitatively correct. To demonstrate this, we plot on Fig. 6 two more sets of

calculated values, obtained by using extremely large lower and upper bounds for the order parameter variation in the $N_{TB}$ phase. As a lower limit we suppose that the order parameter jumps at the transition by $\delta S^{TB}$, the smallest possible jump compatible with the measured value of $\delta n_W$, and then remains constant throughout the twist-bend phase, $S^{TB}_{min}(T) = \delta S^{TB} + S^{N}(T_{NtbN})$. For the upper limit we assume that the jump at the transition is twice as large, $2\delta S^{TB}$, and that at $T < T_{NtbN}$ the variation of the order parameter follows the trend of the curve extrapolated from the N-phase, $S^{TB}_{max}(T) = 2\delta S^{TB} + S^{N}_{extr}(T)$. Although both these assumptions are drastically exaggerated, the curve $\theta(T)$ remains relatively stable, with respectively a 10 % decrease of $\theta$ at low temperatures, or an increase of $\theta(T_{NtbN})$ by about 4°.

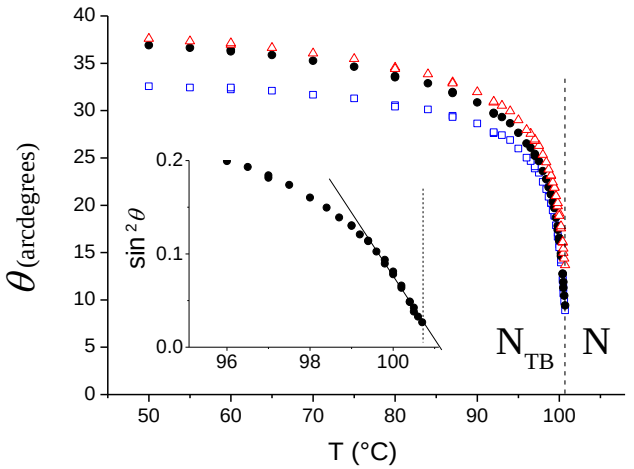


**Fig. 6** Temperature dependence of the heliconical angle throughout the supercooled $N_{TB}$ phase of CB7CB, calculated from the birefringence measurements in the single-domains (full black points). The open symbols, blue squares and red triangles are respectively the lower and upper bounds for $\theta(T)$, obtained when assuming drastically different approximations for the order parameter variation in the $N_{TB}$ phase. In the inset is shown the temperature dependence of $\sin^2\theta$ in the vicinity of the transition. The first few points fit well with the theoretically expected linear law [14].

### Structure of the defect walls

One of the most unexpected results in the present work is the temperature dependence of $\Delta n$ measured in the walls between the chiral monodomains with opposite handedness. Indeed, it is drastically different from the curve extrapolated from the N-phase and that measured in the monodomains. This discrepancy cannot be explained by the lower precision of the direct measurement of $\Delta n_W$ with the Berek compensator, despite its larger error bars. To understand this result we need to consider the possible structure of the defects separating the doubly degenerate $N_{TB}$ monodomains. A detailed description of these defects and estimation of their energy is far beyond the scope of the present work. However, our data does provide sufficient information for the qualitative discussion of the observed defect walls.

Let us consider two perfectly ordered $N_{TB}$ domains with opposite twist-bend handedness, in contact between them on a plane perpendicular to the pitch axis **Z** (see Fig. 7). Each of these domains corresponds to the doubly degenerate energy minimum of the $N_{TB}$ distortion energy, with a spontaneously bent nematic director, **n**. However, there is no smooth passage from one domain to the other with conservation of the spontaneous bend at its optimal value, i.e. the two minima are separated in the "phase-space" of the system by higher energy intermediary states. We may expect then some defects in the region where the sign inversion of the chirality takes place. This situation is somewhat similar to the usual case of nematic or smectic liquid crystals subject to constraints imposed by boundary conditions or external fields. Typically, these constraints are resolved by introducing line-defects (less costly than plane-defects), disclinations or dislocations, with respectively the orientational or translational order destroyed in their core. However, despite the close analogy between the nematic, smectic and the $N_{TB}$ phases, to realize the defect wall that we are interested in here, we do not need to destroy the nematic order in the defect cores. Strictly speaking we do not need any defects in the tensor field of the nematic order parameter, **Q**, but only defects of the "order parameters" describing the $N_{TB}$ - N phase transition, e.g. the tilt angle $\theta$ [14]. Moreover, it is easy to see that there are several possible ways to invert the sign of the chirality between the two domains by a smooth, one-dimensional variation of the $N_{TB}$ structure, without changing the nematic order parameter (see Fig. 7). We note that the resulting planar defect, or defect wall, is similar to the "melted grain boundary" defects proposed for the smectic A and smectic C phases in the vicinity of the phase transition [39, 40].

Fig. 7 presents the different possible structures of the defect walls. In all of the cases the wall connects two adjacent monodomains of the $N_{TB}$ phase with opposite handedness and with the helix axis parallel to **Z**. Further all of the variables are functions only of the coordinate *Z*. In the first structure, shown on Fig. 7a, the tilt angle remains constant, at its equilibrium value, and only the "phase" $\varphi$ of the heliconical distortion varies along *Z*. In the monodomains the pitch is $q = d\varphi/dZ = \pm q_s$, the spontaneous pitch of the helix, and between them it increases gradually from $-q_s$ on the left to $+q_s$ on the right. In the middle of the wall $q=0$ and the spontaneous bend vanishes completely: the structure there corresponds in fact to the usual undistorted nematic phase N and not to the spontaneously distorted twist-bend nematic. The excess energy density of the nematic "core" of the defect is $f_N - f_{TB} = -K_3^3/(54CK_2)$, where *C* is the fourth order elastic constant of the bent-shape nematic [14]. The effective rotational symmetry of the $N_{TB}$ phase is broken in the center of the wall – the optical axis there is along the local direction of **n** and not along the helix axis. In the bulk the projection of **n** on the **XY** plane, $\mathbf{n}_\perp$, is arbitrary oriented, but this degeneracy is broken on the boundary surfaces, parallel to the **YZ** plane. In fact, the imposed surface anchoring is as usual anisotropic, with out-of-plane anchoring energy much stronger than the in-plane one and the director will prefer to orient in the **YZ** plane. Then, in the geometry of our experiment, with the light propagating along **X**, we should observe a rotation of the local optical axis in the middle of the wall at angle $\pm\theta$ with respect to the helix axis **Z**. However, no such deviation was observed in our POM experiment, very sensitive as it is to the in-plane deviation of the optical axis, and so we can conclude that this first scenario, a circular heliconical standing wave of the director **n** with a variable wavelength, does not explain the structure of the defect walls.

The second possible structure is presented in Fig. 7b. In this case the wave vector modulus $|q|$ remains constant throughout the

wall, $|q| = |q_s|$, but $\theta$ decreases, changes sign in the center of the wall, and then increases again to its temperature-equilibrium value. We note that at $\theta = 0$ the wave vector $d\varphi/dZ$ can change sign, enabling it to invert the handedness of the adjacent monodomains without introducing a singularity of the director field. Once more the nematic is uniform in the middle of the wall and the excess energy density in the defect "core" is the same as before, namely $-K_3^3/(54CK_2)$. In this case the optical axis remains parallel to **Z** everywhere, in the wall and in the monodomains, and we cannot discriminate this structure by simple POM observations. However, the birefringence in the uniform region should be the same as the nematic birefringence at the same temperature, i.e. close to the extrapolated value $S^{N}_{extr}(T)$. This is in drastic disagreement with the results plotted on Fig. 5 and so we can also reject the second scenario, circular heliconical standing wave of the director, **n**, with variable conical tilt angle.

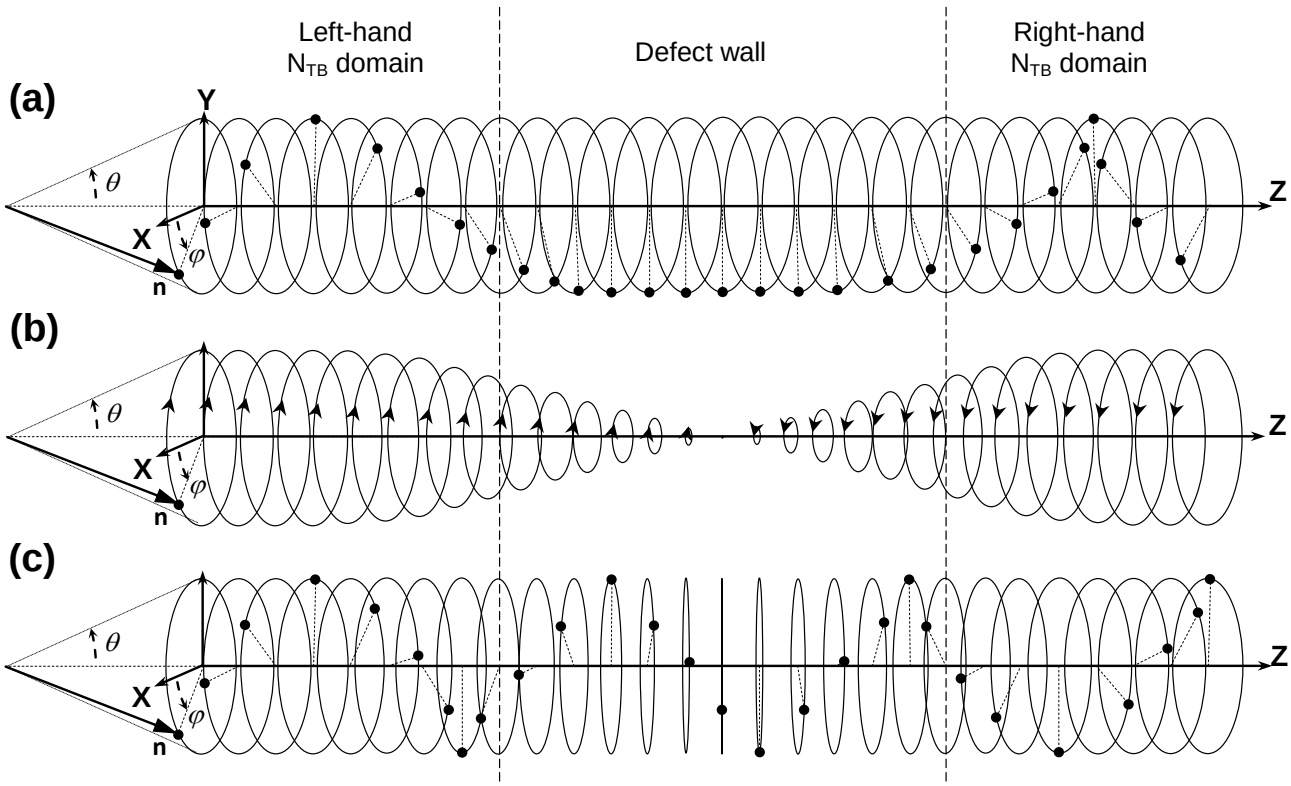


**Fig. 7** Possible structures of the planar defect separating the monodomains of the $N_{TB}$ phase having opposite handedness. In the chiral monodomains the projection $\mathbf{n}_\perp$ of the director on the **XY**-plane forms a circularly polarized standing wave with wavevector $q=d\varphi/dZ$, with respectively left- or right-handed polarization on the left and right sides of the figure. In (a) and (c) the projection $\mathbf{n}_\perp$ is shown with a dashed line and the position of **n** on the twist-bend cone is indicated with a full point; in (b), for simplicity, only the direction of the rotation of **n** on the cone is shown. Three distinct structures of the defect are considered: (a) The circularly polarized standing wave with constant aperture of the cone, $\theta$, and continuously variable wavevector $q$. In the defect "core" $q$=0, **n** is uniform and tilted at the angle $\theta$ with respect to **Z**; (b) The circularly polarized standing wave with continuously variable aperture of the cone and constant wavevector. In the defect "core" **n** is uniform and parallel to **Z**; (c) The elliptically polarized wave with continuously variable axial ratio of the elliptical cone and constant wave vector. In the defect "core" **n** oscillates in the **YZ**-plane as predicted for the splay-bend nematic phase.

The third possibility is sketched on Fig. 7c. In this case the standing wave of the director in the wall no longer has circular polarization, but becomes elliptical. In the middle of the wall it is even linearly polarized, enabling the inversion of the sign of the chirality. We note that in the center of the wall the structure is not uniform, as for the other two cases, but similar to the director distortion in the splay-bend nematic phase, $N_{SB}$. This phase has been predicted as another spontaneously distorted nematic phase[14], taking place when the elastic constant $K_3$ becomes negative, realized instead of the $N_{TB}$ phase when $K_1 < 2K_2$. The defect wall with this induced $N_{SB}$ structure at its "core" has an excess energy density[14] $f_{SB} - f_{TB} = \frac{K_3^3}{54C}\left(\frac{2}{K_1} - \frac{1}{K_2}\right)$ with respect to the thermodynamically stable $N_{TB}$ phase. Taking into account the observation that usually $K_1$ is not much larger than $2K_2$, this energy is significantly smaller than the energy density of the defect wall with a uniform-nematic "core". We then expect that the structure of the observed defect walls is similar to that given in Fig. 7c. We note that for the same anchoring reasons discussed previously, in the linearly polarized central region of the defect the director will remain parallel to the **YZ** plane.

To estimate the birefringence of the wall we apply to the $N_{SB}$ phase the approach developed previously for the $N_{TB}$ phase. We start with the same molecular polarizability of the dimer, $\boldsymbol{\alpha}$, and we assume that the order parameter is essentially the same in the $N_{TB}$ and $N_{SB}$ phases. Our reason for this assumption is that, at a given temperature, the Gibbs free energy difference between the twist-bend and nematic phases, $f_{TB} - f_N$, and between the splay-bend and nematic phases, $f_{SB} - f_N$, are expected to be very similar.

In the director frame **123** we obtain

$$\langle \Delta\alpha \rangle^{SB}(T) \approx \Delta\alpha^{m}\left(3\cos^2\psi - 1\right) S^{SB}(T) \approx \Delta\alpha_0^{N} S^{TB}(T). \quad (15)$$

In the $N_{SB}$ phase the local director **n**, parallel to the **3**-axis of the director frame **123**, oscillates periodically in the plane **YZ** of the laboratory frame, $\mathbf{n} \approx (0, \sin(\theta_{SB}\sin(qZ)), \cos(\theta_{SB}\sin(qZ)))$, where $\theta_{SB} << 1$ is the amplitude of the splay-bend oscillation angle. Averaging over one period of the oscillation, we obtain for the average polarizability in the middle of the wall

$$\overline{\langle \Delta\alpha \rangle}^{SB}(T) \approx \Delta\alpha_0^{N}\left(1 - \theta_{SB}(T)^2\right) S^{TB}(T). \quad (16)$$

Finally, for the average birefringence in the splay-bend "core" of the defect we obtain

$$\Delta n^{SB}(T) \approx \Delta n_0^{N} S^{TB}(T)\left(1 - \theta_{SB}(T)^2\right). \quad (17)$$

In Fig. 8 we show the temperature dependence of $\theta_{SB}$, estimated from the linear fit of the $\Delta n_W$ data in Fig. 5 under the same assumption as before for the order parameter in the twist-bend nematic phase, $S^{SB}(T) = S^{TB}(T) = \delta S^{TB} + S^{N}_{extr}(T)$. The temperature variation of $\theta_{SB}(T)$ is weaker than for $\theta_{TB}(T)$, and this feature is not very sensitive to the approximations adopted. In contrast, the result $\theta_{SB}(T_{NtbN}) = 0$ is not reliable, because it is due simply to the lower bound $\delta S^{TB} = 0.032$ adopted for the order parameter jump at the transition, determined from the same $\Delta n_W$ data set. In fact, our results for $\theta_{SB}(T)$ are only qualitative and more quantitative discussion requires further development of both the theoretical model and the experimental techniques for the investigation of the spontaneously distorted nematic phases of bent-shape molecules.

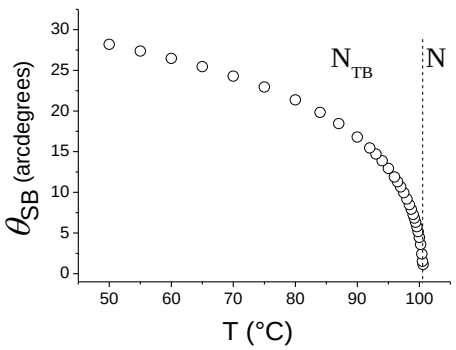


**Fig. 8** Temperature dependence of the tilt angle in the splay-bend "core" of the planar defect wall separating two single-domains of the $N_{TB}$ phase with opposite sign of the chirality.

## Conclusions

In a 1.6 μm sandwich cell with appropriate alignment layers we have achieved almost perfect uniform planar alignment in the two nematic phases, $N_{TB}$ and N, of the bent-shape liquid crystal dimer CB7CB. In the $N_{TB}$ phase we obtain a set of chiral $N_{TB}$ monodomains with alternation of the sign of the chirality, separated by planar defect walls. We have measured precisely the birefringence of the nematic phase and over a range of more than 50 °C in the $N_{TB}$ monodomains. The variation of the birefringence in the $N_{TB}$ phase is smooth and reversible, without hysteresis. This provides strong evidence for the true fluid nematic nature of the $N_{TB}$ phase of CB7CB, instead of a "soft crystal" or "glassy-nematic" state suggested recently[26] for the $N_{TB}$ phase of CB11CB, a compound from the same homologous series of dimers. From the temperature dependence of $\Delta n$, measured in the two nematic phases, we have determined the tilt angle, $\theta_{TB}(T)$, of the heliconical twist-bend structure. At the $N_{TB}$ - N phase transition $\theta_{TB}$ is finite with a value of about 9°, confirming that the transition is weakly first-order. At lower temperatures $\theta_{TB}$ rapidly increases and then almost saturates at about 37°, in qualitative agreement with the negative-elasticity model for the $N_{TB}$ phase.

Although with lower precision, the birefringence is measured also in the defect walls separating the monochiral $N_{TB}$ domains. This birefringence, intermediate between that measured in the monodomains and that expected in the uniform nematic at the same temperature, indicates that in the "core" of the planar defect wall the nematic director is spontaneously distorted and not uniform. We discuss the possible structures of the defect walls and, in qualitative agreement with both our experimental results and the negative-elasticity model, we suggest that the defect presents a splay-bend oscillation of the director. The constraint imposed by the incompatible structures in the single-domains on both sides of the wall induces a transition in the defect from the twist-bend phase to the closely related, although still not observed in thermodynamic equilibrium, splay-bend nematic phase of the bent-shape mesogenic molecules.

## Notes and references

* *Corresponding author*
[a] *Physique des Systèmes Complexes, Université de Picardie Jules Verne, 80039 Amiens, France*
*E-mail: i.dozov@free.fr*
[b] *School of Chemistry, University of Southampton, Highfield, Southampton SO171BJ, United Kingdom*

1 R. B. Meyer, *Phys. Rev. Lett.*, 1969, **22**, 918-921.
2 T. Niori, T. Sekine, J. Watanabe, T. Furukawa and H. Takezoe, *J. Mater. Chem.*, 1996, **6**, 1231-1233.
3 T. Sekine, T. Niori, J. Watanabe, T. Furukawa, S. W. Choi and H. Takezoe, *J. Mater. Chem.*, 1997, **7**, 1307-1309.
4 G. Pelzl, A. Eremin, S. Diele, H. Kresse and W. Weissflog, *J. Mater. Chem.*, 2002, **12**, 2591-2593.
5 V. Goertz, C. Southern, N. W. Roberts, H. F. Gleeson and J. W. Goodby, *Soft Matter*, 2009, **5**, 463-471.
6 C. Prasang, A. C. Whitwood and D. W. Bruce, *Chem. Commun.*, 2008, 2137-2139.
7 M. Sepelj, A. Lesac, U. Baumeister, S. Diele, H. L. Nguyen and D. W. Bruce, *J. Mater. Chem.*, 2007, **17**, 1154-1165.
8 V. P. Panov, M. Nagaraj, J. K. Vij, Y. P. Panarin, A. Kohlmeier, M. G. Tamba, R. A. Lewis and G. H. Mehl, *Phys.Rev. Lett.*, 2010, **105**, 167801.
9 R. A. Reddy and C. Tschierske, *J. Mater. Chem.*, 2006, **16**, 907-961.
10 M. Cestari, S. Diez-Berart, D. A. Dunmur, A. Ferrarini, M. R. de la Fuente, D. J. B. Jackson, D. O. Lopez, G. R. Luckhurst, M. A. Perez-Jubindo, R. M. Richardson, J. Salud, B. A. Timimi and H. Zimmermann, *Phys. Rev. E*, 2011, **84**, 031704.
11 R. B. Meyer, in *Molecular Fluids*, eds. R. Balian and G. Weill, Gordon and Breach, New York 1976, vol. XXV-1973 of *Les Houches Summer School in Theoretical Physics*, pp. 273-373.
12 V. L. Lorman and B. Mettout, *Phys. Rev. Lett.*, 1999, **82**, 940-943.
13 V. L. Lorman and B. Mettout, *Phys. Rev. E*, 2004, **69**, 061710.
14 I. Dozov, *Europhys. Lett.*, 2001, **56**, 247-253.

15 R. Memmer, *Liq. Cryst.*, 2002, **29**, 483-496.
16 C. Meyer, G. R. Luckhurst and I. Dozov, *Phys. Rev. Lett.*, 2013, **111**, 067801.
17 D. Chen, J. H. Porada, J. B. Hooper, A. Klittnick, Y. Shen, M. R. Tuchband, E. Korblova, D. Bedrov, D. M. Walba, M. A. Glaser, J. E. Maclennan and N. A. Clark, *PNAS*, 2013, **110**, 15931-15936.
18 V. Borshch, Y. K. Kim, J. Xiang, M. Gao, A. Jakli, V. P. Panov, J. K. Vij, C. T. Imrie, M. G. Tamba, G. H. Mehl and O. D. Lavrentovich, *Nat. Commun.*, 2013, **4**, 2635-2642.
19 C. Greco, G. R. Luckhurst and A. Ferrarini, *Phys. Chem. Chem. Phys.*, 2013, **15**, 14961-14965.
20 M. Cestari, E. Frezza, A. Ferrarini and G. R. Luckhurst, *J. Mater. Chem.*, 2011, **21**, 12303-12308.
21 K. Adlem, M. Copic, G. R. Luckhurst, A. Mertelj, O. Parri, R. M. Richardson, B. D. Snow, B. A. Timimi, R. P. Tuffin and D. Wilkes, *Phys. Rev. E*, 2013, **88**, 022503.
22 L. Beguin, J. W. Emsley, M. Lelli, A. Lesage, G. R. Luckhurst, B. A. Timimi and H. Zimmermann, *J. Mater. Chem. B*, 2012, **116**, 7940-7951.
23 G. R. Luckhurst, *Macromolecular Symposia*, 1995, **96**, 1-26.
24 V. Fréedericksz and V. Zolina, *Trans. Faraday Soc.*, 1933, **29**, 919-930.
25 Y. P. Bobylev and S. A. Pikin, *Zh. Eksp. Teor. Fiz.*, 1977, **72**, 369-374.
26 R. J. Mandle, E. J. Davis, C. T. Archbold, S. J. Cowling and J. W. Goodby, *J. Mater. Chem. C*, 2014, **2**, 556-566.
27 I. Haller, *Prog. Solid State Chem.*, 1975, **10**, 103-118.
28 S. M. Shamid, S. Dhakal and J. V. Selinger, *Phys. Rev. E*, 2013, **87**, 052503.
29 G. R. Luckhurst, C. Zannoni, P. L. Nordio and U. Segre, *Mol. Phys.*, 1975, **30**, 1345-1358.
30 J. P. Straley, *Phys. Rev. A*, 1974, **10**, 1881-1887.
31 A. Saupe, *Z. Naturforsch. A*, 1964, **19a**, 161.
32 P. G. de Gennes and J. Prost, *The Physics of Liquid Crystals*, Clarendon, Oxford, 1994.
33 G. R. Luckhurst, S. Naemura, T. J. Sluckin, K. S. Thomas and S. S. Turzi, *Phys. Rev. E*, 2012, **85**, 031705.
34 R. Rosso, *Liq. Cryst.*, 2007, **34**, 737-748.
35 M. F. Vuks, *Opt. Spectrosc.*, 1966, **21**, 383.
36 S. T. Wu, *J. Appl. Phys.*, 1991, **69**, 2080-2087.
37 J. Li and S. T. Wu, *J. Appl. Phys.*, 2004, **96**, 6253-6258.
38 S. Roskilly, Ph. D. Thesis, University of Southampton, 1994.
39 I. Dozov, *Phys. Rev. Lett.*, 1995, **74**, 4245-4248.
40 I. Dozov and G. Durand, *Europhys. Lett.*, 1994, **28**, 25-30.